# Selective Interactions of Cationic Porphyrins with G-Quadruplex Structures

**Haiyong Han,[†,‡] David R. Langley,[§] Anupama Rangan,[||] and Laurence H. Hurley*[,†,‡,||]**

*Contribution from the Program in Molecular Biology, The University of Texas at Austin, Austin, Texas 78712, Pharmaceutical Research Institute, Bristol-Myers Squibb Company, 5 Research Parkway, P.O. Box 5100, Wallingford, Connecticut 06492-7660, and Division of Medicinal Chemistry, The University of Texas at Austin, Austin, Texas 78712*

*Received June 19, 2000*

**Abstract:** G-quadruplex DNA presents a potential target for the design and development of novel anticancer drugs. Because G-quadruplex DNA exhibits structural polymorphism, different G-quadruplex typologies may be associated with different cellular processes. Therefore, to achieve therapeutic selectivity using G-quadruplexes as targets for drug design, it will be necessary to differentiate between different types of G-quadruplexes using G-quadruplex-interactive agents. In this study, we compare the interactions of three cationic porphyrins, TMPyP2, TMPyP3, and TMPyP4, with parallel and antiparallel types of G-quadruplexes using gel mobility shift experiments and a helicase assay. Gel mobility shift experiments indicate that TMPyP3 specifically promotes the formation of parallel G-quadruplex structures. A G-quadruplex helicase unwinding assay reveals that the three porphyrins vary dramatically in their abilities to prevent the unwinding of both the parallel tetrameric G-quadruplex and the antiparallel hairpin dimer G-quadruplex DNA by yeast Sgs1 helicase (Sgs1p). For the parallel G-quadruplex, TMPyP3 has the strongest inhibitory effect on Sgs1p, followed by TMPyP4, but the reverse is true for the antiparallel G-quadruplex. TMPyP2 does not appear to have any effect on the helicase-catalyzed unwinding of either type of G-quadruplex. Photocleavage experiments were carried out to investigate the binding modes of all three porphyrins with parallel G-quadruplexes. The results reveal that TMPyP3 and TMPyP4 appear to bind to parallel G-quadruplex structures through external stacking at the ends rather than through intercalation between the G-tetrads. Since intercalation between G-tetrads has been previously proposed as an alternative binding mode for TMPyP4 to G-quadruplexes, this mode of binding, versus that determined by a photocleavage assay described here (external stacking), was subjected to molecular dynamics calculations to identify the relative stabilities of the complexes and the factors that contribute to these differences. The $\Delta G°$ for the external binding mode was found to be driven by $\Delta H°$ with a small unfavorable $T\Delta S°$ term. The $\Delta G°$ for the intercalation binding model was driven by a large $T\Delta S°$ term and complemented by a small $\Delta H°$ term. One of the main stabilizing components of the external binding model is the energy of solvation, which favors the external model over the intercalation model by −67.94 kcal/mol. Finally, we propose that intercalative binding, although less favored than external binding, may occur, but because of the nature of the intercalative binding, it is invisible to the photocleavage assay. This study provides the first experimental insight into how selectivity might be achieved for different G-quadruplexes by using structural variants within a single group of G-quadruplex-interactive drugs.

## Introduction

G-quadruplexes are four-stranded DNA structures formed from stacked guanine tetrads. DNA oligomers with two or more G-clusters are usually able to form multiple G-quadruplex structures that can be classified into either parallel or antiparallel quadruplexes. Scheme 1 shows examples of G-quadruplexes that can form from oligomers that have two three-guanine clusters. The guanines in a parallel-stranded G-quadruplex (Scheme 1a) in which four DNA strands associate together with the same 5′- to 3′-orientation uniformly adopt the same anti glycosidic conformation.[1] This guanine arrangement produces four identical grooves that are about the same size as the minor groove of B-DNA.[2] In antiparallel G-quadruplexes (Scheme 1b−d), two DNA strands run in orientations opposite to the other two strands. The strands that run in the same orientation can be either adjacent (Scheme 1b,d) or nonadjacent (diagonal) (Scheme 1c).[3] The glycosidic torsional angles within a tetrad or along a guanine strand can be the same (all syn or anti) or mixtures of anti/syn conformations. In contrast to parallel-stranded G-quadruplexes, the four grooves in an antiparallel quadruplex are not identical. For example, dimeric hairpin G-quadruplexes with loops joining the two G-clusters on the same end of the G-quadruplex (Scheme 1c) have two medium grooves and two narrow grooves,[4] whereas those with loops joining the two G-clusters across the diagonal (Scheme 1b) have one wide groove, two

* Address correspondence to this author. Tel: 520 626-5622. Fax: 520 626-5623. E-mail: hurley@pharmacy.arizona.edu.

† Program in Molecular Biology, The University of Texas at Austin.

‡ Current address: College of Pharmacy and Arizona Cancer Center, The University of Arizona, Tucson, AZ 85724.

§ Bristol-Myers Squibb Co.

|| Division of Medicinal Chemistry, The University of Texas at Austin.

(1) Wellinger, R. J.; Sen, D. *Eur. J. Cancer* **1997**, *33*, 735−749.

(2) (a) Wang, Y.; Patel, D. J. *Biochemistry* **1992**, *31*, 8112−8119. (b) Wang, Y.; Patel, D. J. *J. Mol. Biol.* **1993**, *234*, 1171−1183.

(3) Wang, Y.; Patel, D. J. *Structure* **1994**, *2*, 1141−1156.

(4) Kang, C.; Zhang, X., Ratliff, R; Moyzis, R; Rich, A. *Nature* **1992**, *356*, 126−131.

10.1021/ja002179j CCC: $20.00 
Published on Web 08/23/2001

**Scheme 1**[a]

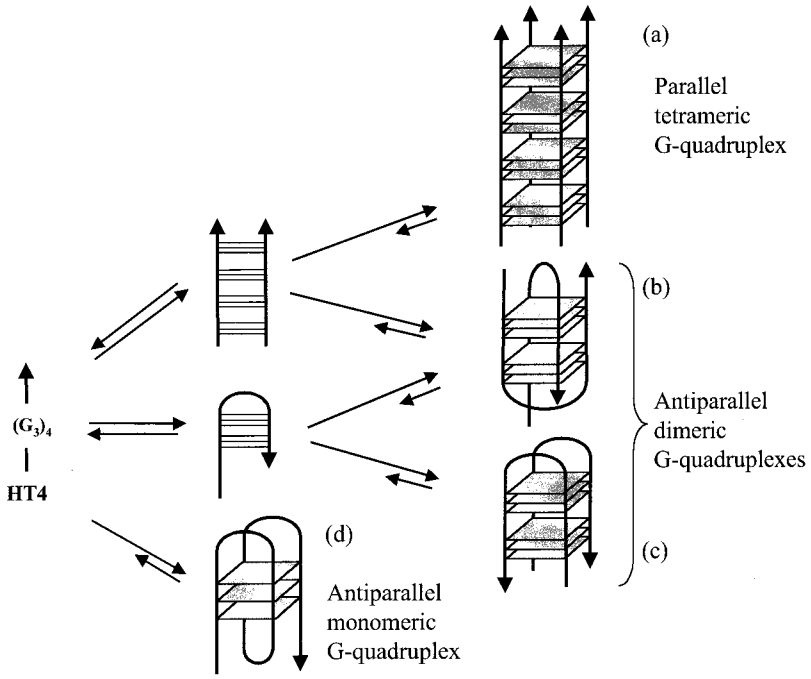


[a] Schematic diagram showing the formation of different types of G-quadruplex structures by an oligomer containing two three-guanine clusters, such as the HT4 sequence. Structures b and c are shown as representative examples of possible dimeric G-quadruplexes formed by HT4. Structure d is an example from a set of different intramolecular G-quadruplexes that might be formed by HT4. For detailed discussion of different types of G-quadruplex structures, refer to refs 2 and 7.

medium grooves, and one narrow groove.[5] Foldover monomeric G-quadruplexes with diagonal loops also have one wide groove, two medium grooves, and one narrow groove (Scheme 1d).[6] Consequently, depending on DNA sequence and the arrangement of strand orientations, the groove sizes vary among different antiparallel G-quadruplexes, which may provide the structural diversities needed for specific G-quadruplex recognition.[2,7] Since G-quadruplex-interactive compounds generally bind by stacking externally to the G-tetrads, the structures of loops and adjacent non-G-tetrads might also influence binding specificity.

It is the loop regions that potentially have the most topological variations. Therefore, ligands that interact externally to the G-tetrad structure are the most attractive to gain selectivity. Small organic molecules have been proposed to be able to interact noncovalently with G-quadruplex through G-tetrad stacking, groove binding, loop binding, and intercalation between two G-tetrads. The only G-quadruplex−small molecule complex structure solved so far by $^1$H NMR showed that PIPER, a perylene analogue, stacks externally to the G-tetrads at the ends of G-quadruplexes.[8] In a recent study, Read and Neidle proposed that 1,4-bis(piperidino)amidoanthraquinones also stack externally to the G-tetrads, based on molecular modeling and fiber diffraction studies.[9]

Recently, many genomic regions, including telomeres,[10] the dimerization region of HIV,[11] the regulatory region of the insulin gene,[12] fragile X-syndrome triplet repeats,[13] and the promoter region of the c-*myc* gene,[14] have been proposed to form G-quadruplex structures in cell-free systems. We recently demonstrated that PIPER is able to facilitate the formation of G-quadruplex structures from duplex DNA.[15] Topoisomerase I has also been recently shown to facilitate the formation of G-quadruplex structures.[16] Although the in vivo existence of G-quadruplex structures has yet to be proven, G-quadruplex DNA has been suggested as a potential target for the development of novel anticancer agents.[17] To date, several groups of G-quadruplex-interactive agents have been shown to have in vitro antitumor activities.[18,19] Since G-quadruplex DNA exhibits

(5) Smith, F. W.; Feigon, J. *Nature* **1992**, *356*, 164−168.
(6) (a) Wang, Y.; Patel, D. J. *Structure* **1993**, *1*, 263−282. (b) Wang, Y.; Patel, D. J. *J. Mol. Biol.* **1995**, *251*, 76−94.
(7) Williamson, J. R. *Annu. Rev. Biophys. Biomol. Struct.* **1994**, *23*, 703−730.
(8) Fedoroff, O. Yu.; Salazar, M.; Han, H.; Chemeris, V. V.; Kerwin, S. M.; Hurley, L. H. *Biochemistry* **1998**, *37*, 12367−12374.
(9) Read, M. A.; Neidle, S. *Biochemistry* **2000**, *39*, 13422−13432.
(10) Henderson, E.; Hardin, C. C.; Walk, S. K.; Tinoco, I., Jr.; Blackburn, E. H. *Cell* **1987**, *51*, 899−908.
(11) Sundquist, W. I.; Heaphy, S. *Proc. Natl. Acad. Sci. U.S.A.* **1993**, *90*, 3393−3397.
(12) Hammond-Kosack, M. C.; Kilpatrick, M. W.; Docherty, K. *J. Mol. Endocrinol.* **1992**, *9*, 221−225.
(13) (a) Nadel, Y.; Weisman-Shomer, P.; Fry, M. *J. Biol. Chem.* **1995**, *270*, 28970−28977. (b) Fry, M.; Loeb, L. A. *Proc. Natl. Acad. Sci. U.S.A.* **1994**, *91*, 4950−4954.
(14) Simonsson, T.; Pecinka, P.; Kubista, M. *Nucleic Acids Res.* **1998**, *26*, 1167−1172.
(15) Rangan, A.; Fedoroff, O. Yu.; Hurley, L. H. *J. Biol. Chem.* **2001**, *276*, 4640−4646.
(16) Arimondo, P. B.; Riou, J.-F.; Mergny, J.-L.; Tazi, J.; Sun, J.-S.; Garestier, T.; Hélène, C. *Nucleic Acids Res.* **2000**, *28*, 4832−4838.
(17) (a) Hurley, L. H. *J. Med. Chem.* **1989**, *32*, 2027−2033. (b) Mergny, J. L.; Hélène, C. *Nat. Med.* **1998**, *4*, 1366−1367. (c) Mergny, J. L.; Mailliet, P.; Lavelle, F.; Laoui, A.; Hélène, C. *Anti-Cancer Drug Des.* **1999**, *14*, 327−339. (d) Han, H.; Hurley, L. H. *Trends Pharm. Sci.* **2000**, *21*, 136−142. (e) Kerwin, S. M. *Curr. Pharm. Des.* **2000**, *6*, 441−478. (f) Neidle, S.; Kelland, L. R. *Anti-Cancer Drug Des.* **2000**, *13*, 341−347. (g) Sun, D.; Thompson, B.; Cathers, B. E.; Salazar, M.; Kerwin, S. M.; Trent, J. O.; Jenkins, T. C.; Neidle, S.; Hurley, L. H. *J. Med. Chem.* **1997**, *40*, 2113−2116.
(18) (a) Raymond, E.; Sun, D.; Chen, S. F.; Windle, B.; Von Hoff, D. D. *Curr. Opin. Biotechnol.* **1996**, *7*, 583−591. (b) Sharma, S.; Raymond, E.; Soda, H.; Sun, D.; Hilsenbeck, S. G.; Sharma, A.; Izbicka, E.; Windle, B.; Von Hoff, D. D. *Ann. Oncol.* **1997**, *8*, 1063−1074. (c) Wheelhouse, R. T.; Sun, D.; Han, H.; Han, F. X.; Hurley, L. H. *J. Am. Chem. Soc.* **1998**, *120*, 3261−3262. (d) Izbicka, E.; Wheelhouse, R. T.; Raymond, E.; Davidson, K. K.; Lawrence, R. A.; Sun, D.; Windle, B. E.; Hurley, L. H.; Von Hoff, D. D. *Cancer Res.* **1999**, *59*, 639−644.

**Chart 1**

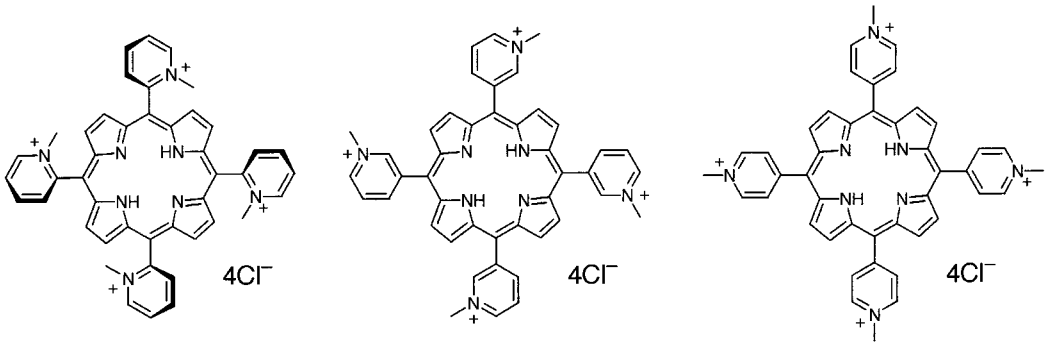


**TMPyP2** **TMPyP3** **TMPyP4**

polymorphism, to achieve specificity it is critical for G-quadruplex-interactive agents to selectively facilitate the formation of specific complexes or to interact with different types of G-quadruplexes to selectively inhibit G-quadruplex helicases. Thus, the relative dynamics of specific G-quadruplex formation and their relative stability to helicase in the presence of G-quadruple-interactive compounds could be the basis for selectivity of ligands that interact with G-quadruplex structures. We previously proposed that the contrasting telomerase inhibitory activities of two positional porphyrin isomers, 5,10,15,20-tetra(*N*-methyl-2-pyridyl)porphine (TMPyP2) and 5,10,15,20-tetra(*N*-methyl-4-pyridyl)porphine (TMPyP4), are due to their different interactive modes with intramolecular foldover G-quadruplex.[20] In this report, we compare the relative dynamics of formation and stabilization to helicase unwinding of parallel and antiparallel tetrameric G-quadruplexes using three positional cationic porphyrin isomers, TMPyP2, 5,10,15,20-tetra(*N*-methyl-3-pyridyl)porphine (TMPyP3), and TMPyP4 (Chart 1). Using photocleavage methods, we demonstrate that TMPyP3 has the apparent strongest binding affinity with parallel G-quadruplexes, followed by TMPyP4 with moderate activity, whereas TMPyP2 has almost no interaction with these structures. We also provide additional molecular dynamics calculations that predict that the favored manner for TMPyP4 binding with the monomolecular, antiparallel G-quadruplex is by external stacking rather than by the inter-G-tetrad intercalative model that was previously proposed by Haq and co-workers in a parallel G-quadruplex structure.[21] However, on the basis of the stoichiometry of binding of TMPyP4 to this same G-quadruplex determined by this same group, we propose that an additional TMPyP4 molecule might bind by an intercalative mode but that the expected photocleavage is quenched by this mode of binding.

## Materials and Methods

**Helicase, Oligonucleotide, and Porphyrin Preparation.** A recombinant SGS1 fragment (amino acids 400−1268 of the 1447-amino acid full-length protein) was overexpressed in yeast and purified as described.[22] DNA oligomers (Scc-T, 5′-AACTTGTGTGGGTGTGTGTGTGGGTGTGTGT-3′;OX1-T,5′-ACTGTCGTACTTGATATTTTGGGGTTTTGGGGAATGTGA-3′;[23] $H_1$, 5′-$(T)_{30}$GCTAGTTGGGAAGCCGATGC-3′; $K_1$, 5′-GCATCGGCTTCCCAACTAGC$(T)_{10}$-3′; and HT4, 5′-TTAGGGTTAGGGTTAGGGTTAGGG-3′) were synthesized on an Expedite synthesizer (PerSeptive Biosystems, model 8909) and purified by denaturing PAGE.

The three porphyrin derivatives TMPyP2, TMPyP3, and TMPyP4 were purchased from Mid-Century Chemicals (Chicago, IL). A 1 mM stock solution in $H_2O$ was prepared for each compound and stored at −20 °C.

**G-Quadruplex DNA Formation.** The formation of G-quadruplex DNA was carried out as described.[23,24] Briefly, 260 $\mu$M Scc-T was denatured in 1× TE (pH 8.0) containing 1 M NaCl or 1 M KCl by heating at 95 °C for 10 min. The denatured DNA was then annealed at 37 °C for 48 h. The annealed products were separated on an 8% native PAGE containing 10 mM KCl. Bands corresponding to tetrameric G-quadruplex, dimeric G-quadruplex, and monomeric Scc-T were excised from the gel and eluted with 1× TE (pH 8.0) containing 50 mM NaCl and 20 mM KCl. The purified G-quadruplex DNA was 5′-$^{32}$P-labeled and purified with native PAGE. Labeled G-quadruplex DNA was precipitated with ethanol and stored in 10 mM Tris-HCl (pH 7.5) containing 100 mM KCl at −20 °C.

**Gel Mobility Shift Assay.** $^{32}$P-Labeled HT4 at a concentration of 8 $\mu$M was annealed by heating to 95 °C for 10 min in 1× TE buffer (pH 8.0) containing 100 mM KCl followed by slow cooling to room temperature.[25] Two microliters of the respective stock solution of porphyrins (TMPyP2, TMPyP3, TMPyP4) was added to each sample to obtain the concentrations shown in the figures. Reaction mixtures were incubated for 8−10 h at room temperature. The reactions were terminated by the addition of 8 $\mu$L of gel loading buffer (30% glycerol, 0.1% bromophenol blue, 0.1% xylene cyanol). Ten microliters of the subsequent solution was analyzed on a 16% native PAGE (the gel was prerun for 30 min). Electrophoresis was carried out for 15 h at 4 °C in 1× TBE buffer (pH 8.3) containing 20 mM KCl. Gels were dried and then visualized on a PhosphorImager (Molecular Dynamics model 445 SI).

**Helicase Assay.** The helicase unwinding assay was performed as described with some modifications.[22,23] About 10 000 counts/min of $^{32}$P-labeled DNA (100 nM) was incubated with TMPyP2, TMPyP3, and TMPyP4 at concentrations indicated in the figures in a helicase reaction buffer (50 mM Tris-HCl (pH 7.5), 2 mM $MgCl_2$, 2 mM ATP, 50 mM NaCl, and 100 $\mu$g/mL BSA) for 30 min at room temperature. Sgs1p, 25 nM, was added to the reactions, which were then incubated at 30 °C for 30 min. Reactions were stopped by adding SDS and proteinase K to final concentrations of 0.5% and 0.5 mg/mL, respectively, and incubating at 37 °C for 10 min. Samples were then separated on an 8% native polyacrylamide gel containing 10 mM KCl. Gels were dried on a dryer and visualized on a PhosphorImager.

**Photocleavage Assay.** Parallel G-quadruplex DNA formed from oligonucleotide Scc-T was labeled with 5′-$^{32}$P and stored in 1× TE (pH 8.0) buffer containing 100 mM KCl. For each photocleavage reaction, ∼30 000 counts/min of DNA was diluted with 100 mM KCl

(19) Perry, P. J.; Kelland, L. R. *Exp. Opin. Ther. Pat.* **1998**, *8*, 1567−1586.
(20) Han, F. X.; Wheelhouse, R. T.; Hurley, L. H. *J. Am. Chem. Soc.* **1999**, *121*, 3561−3570.
(21) Haq, I.; Trent, J. O.; Chowdhry, B. Z.; Jenkins, T. C. *J. Am. Chem. Soc.* **1999**, *121*, 1768−1779.
(22) Bennett, R. J.; Sharp, J. A.; Wang, J. C. *J. Biol. Chem.* **1998**, *273*, 9644−9650.
(23) Sun, H.; Bennett, R. J.; Maizels, N. *Nucleic Acids Res.* **1999**, *27*, 1978−1984.
(24) Sen, D.; Gilbert, W. *Methods Enzymol.* **1992**, *211*, 191−199.
(25) Han, H.; Cliff, C. L.; Hurley, L. H. *Biochemistry* **1999**, *38*, 6981−6986.

to give a final concentration of 1500 counts $min^{-1}$ $\mu L^{-1}$. For denaturing control samples, DNA was diluted with $H_2O$ and boiled for 10 min before cooling down on ice. The diluted DNA was then mixed with 2 $\mu$L of a 1 $\mu$M TMPyP2, TMPyP3, or TMPyP4 solution and transferred to a 96-well microtiter plate. For the time course experiment, porphyrin−DNA mixtures were incubated for the time periods indicated in the figure legend before being transferred to a 96-well plate. The microtiter plate was covered with a glass filter to eliminate UV light under 300 nM and to reduce evaporation. The samples were then exposed to a 24-W fluorescent light for 2, 5, 10, and 20 min or for 15 min for the incubation time course experiments.[20] The reactions were stopped by adding 100 $\mu$L of 0.1 $\mu$g/$\mu$L calf thymus DNA containing 0.3 M sodium acetate. After phenol−chloroform extraction and ethanol precipitation, the samples were subjected to piperidine treatment to induce strand breakage. Finally, the DNA samples were separated on a 16% denaturing polyacrylamide gel and visualized on a PhosphorImager.

**Molecular Modeling.** Eleven nanoseconds of molecular dynamics was used to study the binding mode of TMPyP4 with the antiparallel $d(AG_3[T_2AG_3]_3)$ G-quadruplex (see Figure 7A and B). The calculations were conducted in fully solvated and ionic environments using periodic boundary conditions. These calculations were carried out with CHARMM[26] using the BMS force field.[27]

**Model Building.** The NMR structure of the $d(AG_3[T_2AG_3]_3)$ antiparallel G-quadruplex[6a] (143D.pdb) was used in the modeling studies. Before the structure from 143D.pdb could be used, the chirality of the 2′-deoxyribose for G3 had to be corrected. The corrected structure was placed in a 38.7837-Å$^3$ box with 1747 TIP3P[28] water molecules and 21 potassium ions to neutralize the charge on the phosphate groups. Three ions were placed in the core of the quadruplex[29] between tetrads 1 and 2, tetrads 2 and 3, and tetrad 3 and the lateral loops.[30] The remaining ions were positioned near the phosphate groups located in the tetrad core and in the lateral loops of the G-quadruplex. Each ion was initially placed 6 Å from a phosphate atom along the O5′-P vector.[31] This system will be referred to as the $K^+$ complex (see Figure 7B).

TMPyP4 was constructed in QUANTA (Molecular Simulations Inc.) and placed in the center of a 31.0432-Å$^3$ box with 940 TIP3P[32] water molecules and 4 chloride ions to neutralize the TMPyP4 charge.

The TMPyP4−G-quadruplex complexes (see Figure 7B) were constructed by inserting TMPyP4 into the model discussed above for $d(AG_3[T_2AG_3]_3)$ and removing the four potassium ions closest to the four pyridinium groups of TMPyP4. In addition, the number of water molecules was reduced from 1747 to 1701 to offset the volume of TMPyP4. In the G1 complex, TMPyP4 was placed at the end of the G-quadruplex between tetrad 1 ($G_2$, $G_{10}$, $G_{14}$, $G_{22}$) and the lateral loop (see Figure 7B). In the G2 complex, TMPyP4 was intercalated between tetrad 1 ($G_2$, $G_{10}$, $G_{14}$, $G_{22}$) and tetrad 2 ($G_3$, $G_9$, $G_{15}$, $G_{21}$) (see Figure 7B). The potassium ion that previously occupied this location was moved between tetrad 1 and the diagonal loop.[30]

Each system was prepared for molecular dynamics (MD) simulation in several steps. First, the solvent was relaxed with 2000 steps of adopted basis Newton−Raphson (ABNR) minimization while the solute and ions were held fixed. The solvent and ions were then relaxed around the fixed solute with another 2000 steps of ABNR. Finally, the complete system was minimized with 50 steps of ABNR. Each system was then simulated using molecular dynamics for 2.02 ns for TMPyP4 or 3.02 ns for the $K^+$, G1, and G2 complexes. All calculations were carried out with CHARMM[26] using the BMS force field.[27] The calculations were run on the BMS Cray C90 and SGI cluster (calculation details are given in Supporting Information).

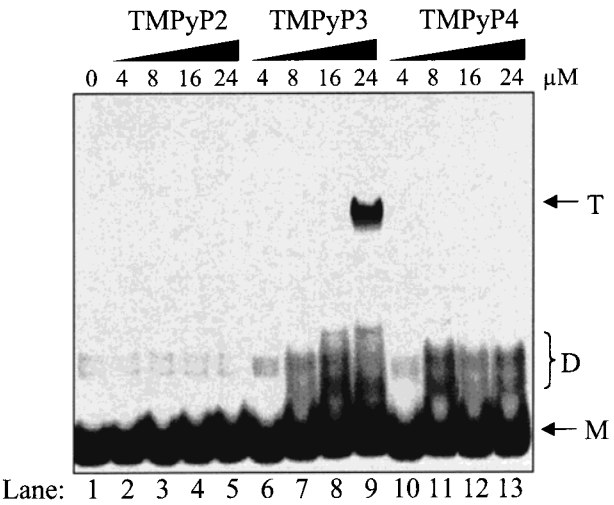


**Figure 1.** Effect of porphyrins on the facilitation of parallel G-quadruplex assembly illustrated by native PAGE. Porphyrins were titrated against HT4 in TE buffer containing 100 mM KCl (lane 1, control; lanes 2−5, TMPyP2; lanes 6−9, TMPyP3; lanes 10−13, TMPyP4). Major bands identified are monomer (M), dimer (D), and tetramer (T).

## Results

**TMPyP3 Specifically Promotes the Formation of Parallel G-Quadruplex Structures.** Native gel electrophoresis was carried out to compare the possible differential effects of the three positional porphyrin isomers in facilitating the formation of parallel and antiparallel G-quadruplex structures. The DNA oligomer used was $d(TTAGGG)_4$ (HT4). This oligomer contains four repeats of the human telomeric sequence and hence has the potential to form both the parallel and antiparallel G-quadruplex structures (Scheme 1). Under the buffer conditions used in the experiment (1× TE, pH 8.0, and 100 mM KCl) and in the absence of porphyrins, HT4 forms several species that are visible in the mobility shift assay (lane 1 in Figure 1). On the basis of previous gel shift data using similar DNA oligomers,[11,25] we designated those species to be dimers (D) and monomers (M) (Figure 1). When HT4 was incubated with increasing concentrations of the three porphyrins, we observed an increased amount of dimers in the presence of TMPyP3 and TMPyP4 but not in the presence of TMPyP2, and most strikingly, a distinct lower mobility species was visible only in the presence of TMPyP3 (designated as T, for tetramer, in Figure 1). The migration position on the gel of species T suggested that the higher mobility species corresponded to parallel G-quadruplex structure. In addition, dimethyl sulfate (DMS) footprinting of both dimer and tetramer was carried out (see Supporting Information). Formation of G-quadruplex requires the involvement of N7 of guanine in the Hoogsteen base pairing. Hence, N7 is not susceptible to DMS modification. The methylation protection pattern of monomer and tetramer bands in comparison to a positive control (denatured HT4) shows that both the monomer and the tetramer are protected; however, the denatured HT4 is susceptible to methylation. This indicates that

(26) Brooks, B. R.; Bruccoleri, R. E.; Olafson, B. D.; States, D. J.; Swaminathan, S.; Karplus, M. J. *J. Comput. Chem.* **1983**, *4*, 187−217.
(27) Langley, D. R. *J. Biomol. Struct. Dyn.* **1998**, *16*, 487−509.
(28) Jorgensen, W. L.; Chandrasekhar, J.; Madura, J. D.; Impey, R. V.; Klein, M. L. *J. Chem. Phys.* **1983**, *79*, 929−935.
(29) (a) Sundquist, W. I.; Klug, A. *Nature* **1989**, *342*, 825−829. (b) Williamson, J. R.; Raghuraman, M. K.; Cech, T. R. *Cell* **1989**, *59*, 871−880. (c) Gilbert, D. E.; Feigon, J. *Curr. Opin. Struct. Biol.* **1999**, *9*, 305−314. (d) Schultze, P.; Hud, N. V.; Smith, F. W.; Feigon, J. *Nucleic Acids Res.* **1999**, *27*, 3018−3028. (e) Hud, N. V.; Schultze, P.; Sklenar, V. S.; Feigon, J. *J. Mol. Biol.* **1999**, *285*, 233−243.
(30) (a) Bouaziz, S.; Kettani, A.; Patel, D. J. *J. Mol. Biol.* **1998**, *282*, 637−652. (b) Kettani, A.; Bouaziz, S.; Gorin, A.; Zhao, H.; Jones, R. A.; Patel, D. J. *J. Mol. Biol.* **1998**, *282*, 619−636.
(31) Ravishanker, G.; Auffinger, P.; Langley, D. R.; Jayaram, B.; Young, M. A.; Beveridge, D. L. *Rev. Comput. Chem.* **1997**, *11*, 317−372.
(32) (a) Borissevitch, I. E.; Gandini, S. C. *J. Photochem. Photobiol. B* **1998**, *43*, 112−120. (b) Anantha, N. V.; Azam, M.; Sheardy, R. D. *Biochemistry* **1998**, *37*, 2709−2714. (c) Arthanari, H.; Bolton, P. H. *Anti-Cancer Drug Des.* **1999**, *14*, 317−326. (d) Arthanari, H.; Basu, S.; Kawano, T. L.; Bolton, P. H. *Nucleic Acids Res.* **1998**, *26*, 3724−3728. (e) Ren, J.; Chaires, J. B. *Biochemistry* **1999**, *38*, 16067−16075.

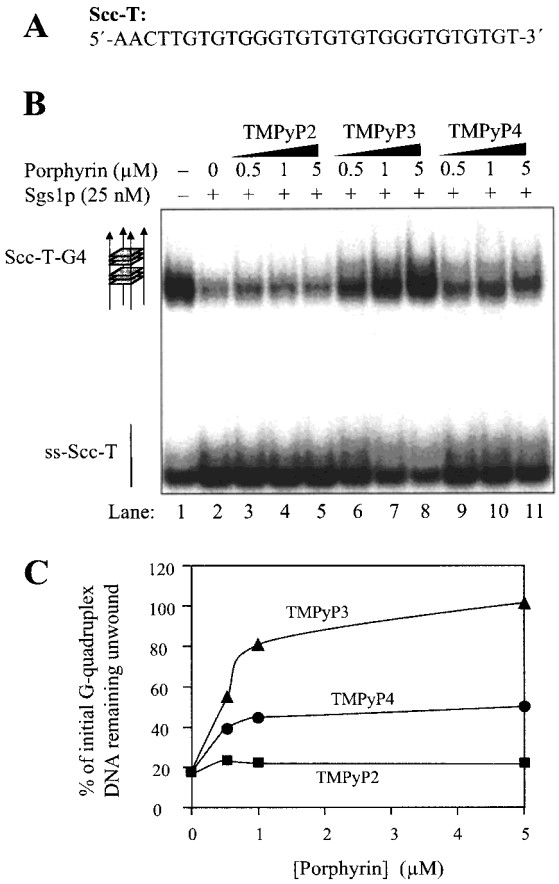


**Figure 2.** Effect of porphyrins on the unwinding of parallel G-quadruplex DNA by helicase. (A) Sequence of Scc-T. (B) About 100 nM tetrameric G-quadruplex DNA (Scc-T−G4) formed from single-stranded Scc-T (ss-Scc-T) was incubated with 25 nM Sgs1p in the presence of increasing amounts of TMPyP2, TMPyP3, and TMPyP4, and products were resolved on an 8% gel. (C) The gel was quantified using ImageQuaNT software (Molecular Dynamics) and the results were graphed as a percentage of initial G-quadruplex DNA to porphyrin concentration.

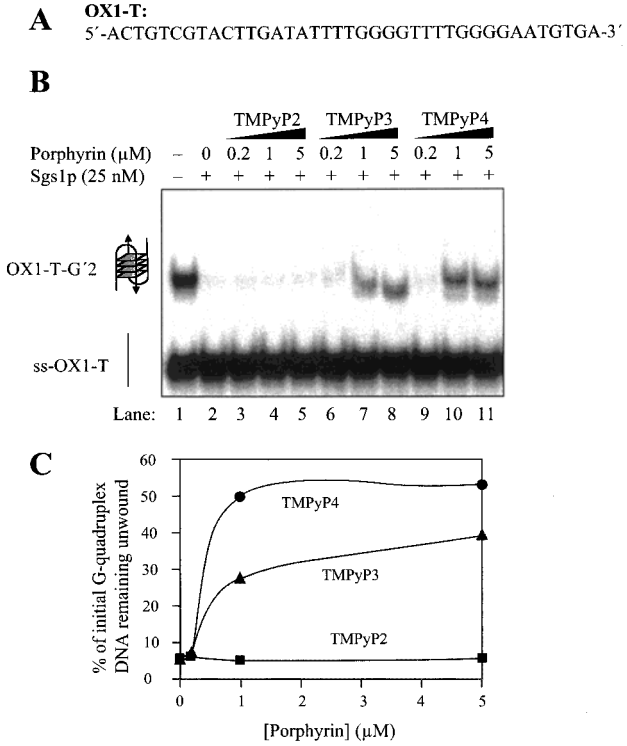


**Figure 3.** Effect of porphyrins on the unwinding of antiparallel G-quadruplex DNA by helicase. (A) Sequence of OX1-T. (B) About 100 nM dimeric G-quadruplex DNA (OX1-T−G′2) formed from single-stranded OX1-T (ss-OX1-T) was incubated with 25 nM Sgs1p in the presence of increasing amounts of TMPyP2, TMPyP3, and TMPyP4, and products were resolved on an 8% gel. (C) The gel was quantified using ImageQuaNT software and the results were graphed as a percentage of initial G-quadruplex DNA to porphyrin concentration.

the monomer might be an intramolecular G-quadruplex structure and the tetramer an intermolecular G-quadruplex structure. Unfortunately, we were unable to collect enough dimeric species to verify their structures by DMS footprinting, although the results of previous studies suggest that they are G-quadruplexes. Most significantly, the results in Figure 1 show that TMPyP3 is unique in facilitating the formation of intermolecular G-quadruplexes.

**TMPyP2, TMPyP3, and TMPyP4 Differentially Prevent the Unwinding of Parallel G-Quadruplex DNA by Sgs1 Helicase.** Cationic porphyrins have been reported to interact with both duplex and quadruplex DNA.[18c,32,33] Porphyrins bind to duplex DNA in many ways, including partial intercalation between base pairs,[33] and they bind to G-quadruplex structures mainly through stacking to G-tetrads.[18c,20,21] However, porphyrins with very similar structures have shown very different binding affinities to antiparallel G-quadruplex DNA.[20] Here we studied the stabilization of parallel G-quadruplexes by cationic porphyrins using a helicase assay. Sgs1p is a yeast helicase that reportedly unwinds G-quadruplex DNA at least 10 times more efficiently than it unwinds duplex DNA.[23] Recently, we have shown that PIPER, a G-quadruplex-interactive compound, can prevent the unwinding of G-quadruplexes by Sgs1 helicase.[34] These features make the Sgs1 helicase unwinding assay a potentially valuable tool to use in studying the differential interactions of G-quadruplex-interactive compounds with G-quadruplexes.

Sgs1 helicase unwinding experiments in the presence of TMPyP2, TMPyP3, and TMPyP4 revealed the different stabilizing effects of these compounds on parallel quadruplex DNA formed from the yeast telomeric sequence Scc-T (Scc-T−G4) (Figure 2). In comparison to control lane 2, in which no porphyrin was added, TMPyP2 had little effect (lanes 3−5), while TMPyP3 showed the highest stabilizing effect on the quadruplex DNA (lanes 6−8), and TMPyP4 had an intermediate effect (lanes 9−11) (Figure 2B). Quantification of gel data in comparison to control lane 1 showed that 5 $\mu$M TMPyP3 maintained 100% of the G-quadruplex, whereas 5 $\mu$M TMPyP4 maintained 50% of the G-quadruplex (Figure 2C).

When a dimeric antiparallel G-quadruplex DNA formed from OX1-T containing two repeats of *Oxytricha* telomeric sequence (OX1-T−G′2) was used in the helicase assay,[23] TMPyP2, TMPyP3, and TMPyP4 again showed different patterns of stabilization (Figure 3). In this case, TMPyP4 had higher stabilizing effects on OX1-T−G′2 than TMPyP3, but consistent with the result using Scc-T−G4, TMPyP2 did not affect the unwinding of OX1-T−G′2 (Figure 3B and C). The differential stabilizations by TMPyP3 and TMPyP4 on Scc-T−G4 and OX1-T−G′2 indicate that the prevention of G-quadruplex unwinding is almost certainly caused by the interaction between G-quadruplex DNA and compounds and not by the interaction

(33) Kruk, N. N.; Dzhagarov, B. M.; Galievsky, V. A.; Chirvony, V. S.; Turpin, P. Y. *J. Photochem. Photobiol. B* **1998**, *42*, 181−190.

(34) Han, H.; Bennett, R. J.; Hurley, L. H. *Biochemistry* **2000**, *39*, 9311−9316.

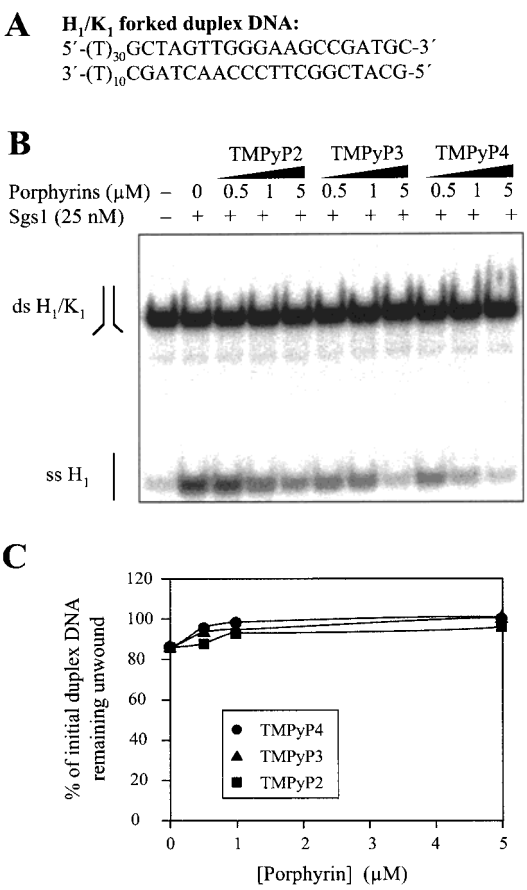


**Figure 4.** Effect of porphyrins on the unwinding of forked duplex DNA $H_1/K_1$ by helicase. (A) Sequence of $H_1/K_1$ duplex. (B) About 100 nM $H_1/K_1$ duplex DNA was incubated with 25 nM Sgs1p in the presence of increasing amounts of TMPyP2, TMPyP3, and TMPyP4, and the products were resolved on an 8% gel. (C) The gel was quantified using ImageQuanNT software, and the results were graphed as a percentage of initial duplex DNA to porphyrin concentration.

between Sgs1 helicase and compounds. The differences among TMPyP2, TMPyP3, and TMPyP4 in their abilities to stabilize the parallel G-quadruplexes suggest that different steric interactions between the pyridyl groups and the porphine nucleus of the porphyrin molecules play an important role in G-quadruplex interactions (see Discussion).

Sgs1 helicase has also been reported to unwind duplex DNA, but with much less efficiency.[23] To compare the effects of different porphyrins on duplex DNA unwinding, we made a forked duplex DNA substrate $H_1/K_1$ for Sgs1p (Figure 4A). The unwinding experiments were carried out in the same way as for the G-quadruplex DNA in the presence or absence of porphyrin analogues. As shown in Figure 4B and C, all three porphyrin analogues showed similar inhibitory activity in $H_1/K_1$ unwinding by Sgs1p. This observation is consistent with the fact that porphyrin analogues interact not only with G-quadruplex DNA but also with duplex DNA.[17g,18c] This pattern of inhibition of Sgs1p is different from those the three porphyrin analogues have on either parallel (Figure 2) or antiparallel (Figure 3) G-quadruplex DNA. The fact that the three porphyrin analogues showed the same inhibitory patterns on duplex DNA but different patterns on different G-quadruplex types is persuasive evidence that the prevention of G-quadruplex DNA unwinding by Sgs1p results from the interaction *between porphyrins and G-quadruplex structures*, not from the interaction between porphyrins and Sgs1p. Although we cannot completely rule out the possibility of such interactions, the interactions between porphyrins and Sgs1 protein are apparently not the major cause of G-quadruplex unwinding inhibition.

**Photocleavage Patterns of TMPyP2, TMPyP3, and TMPyP4 on G-Quadruplex DNA and Their Intensities of Cleavage Parallel Their Different Stabilizing Effects on Different G-Quadruplexes in an Sgs1 Helicase Unwinding Assay.** In an attempt to gain insight into the differences among the various porphyrin analogues observed in the facilitation of the formation of G-quadruplex structures and Sgs1 helicase inhibition, we carried out experiments in which we used the photocleavage potential of the porphyrins to identify both the sites and apparent extents of binding to the G-quadruplex structures. Figure 5 shows the results of the time course of photocleavage of Scc-T−G4 by TMPyP2, TMPyP3, and TMPyP4. All three porphyrins produced an almost uniform level of cleavage on the single-stranded Scc-T at all the guanine residues, particularly those within the two three-guanine clusters (I and II in Figure 5A−C, lanes 3−7). However, when the Scc-T formed the parallel G-quadruplex (Scc-T−G4), which also has two three-guanine clusters (Figure 5D, I and II), the cleavage patterns changed dramatically. TMPyP2 showed almost no cleavage activity against Scc-T−G4 (Figure 5A, lanes 8−12). The result is rather surprising but reproducible. Three possible reasons for this are that (1) under the conditions of the 100 mM $K^+$ buffer, TMPyP2 could not access the guanines, even those located on the outside of the stacking G-tetrads; (2) TMPyP2 is able to bind to the G-tetrads, but the photocleavage is quenched; or (3) TMPyP2 is unable to produce as many free-radical species as those produced in buffers without potassium ions. While TMPyP3 and TMPyP4 showed very strong cleavage with Scc-T−G4, the patterns were quantitatively different from each other and also from those with single-stranded Scc-T (Figure 5B−D). Both TMPyP3 and TMPyP4 strongly cleaved the guanines ($G_8$, $G_{24}$, $G_{26}$) located outside the two guanine clusters and the two guanines located at the 5′-end of guanine cluster I and the 3′-end of guanine cluster II ($G_{10}$ and $G_{22}$, respectively). In comparison to single-stranded Scc-T (ss-Scc-T), the cleavage at guanine residues between $G_{10}$ and $G_{22}$ was greatly reduced for both TMPyP3 and TMPyP4. Guanines located in the middle of the guanine clusters ($G_{11}$, $G_{21}$) were almost completely protected from cleavage by both porphyrins. This result strongly suggests that the porphyrins bind to G-quadruplex structures by stacking to the G-tetrads located at the ends of G-quadruplexes and not by intertetrad intercalation.

According to our photocleavage experiments, binding of porphyrins by noninter-G-tetrad intercalation occurs quite rapidly (i.e., within 2 min; see Figure 5). However, this may not be true for the intercalation of porphyrin molecules *between* two G-tetrads (i.e., intercalation that would result in cleavage at $G_{11}$ and $G_{21}$). We considered the possibility that the binding of porphyrins to the ends of the G-tetrads is *kinetically* favored and the intercalation of porphyrin molecules between two G-tetrads is *thermodynamically* favored. To examine such a possibility, we performed a time course incubation of TMPyP4 with the parallel G-quadruplex before photocleavage. As shown quite clearly in Figure 6, the TMPyP4 photocleavage pattern on Scc-T−G4 DNA *did not change* during the 54-h incubation period. There is no cleavage at the inner G-tetrads ($G_{11}$, $G_{21}$) even after 54 h of incubation. This result apparently argues strongly against the suggestion that G-tetrad intercalation might occur as a thermodynamically driven process.

Interestingly, the cleavages at $G_{14}$, $G_{16}$, and $G_{18}$, which are less likely to be involved in stable G-quadruplex formation,

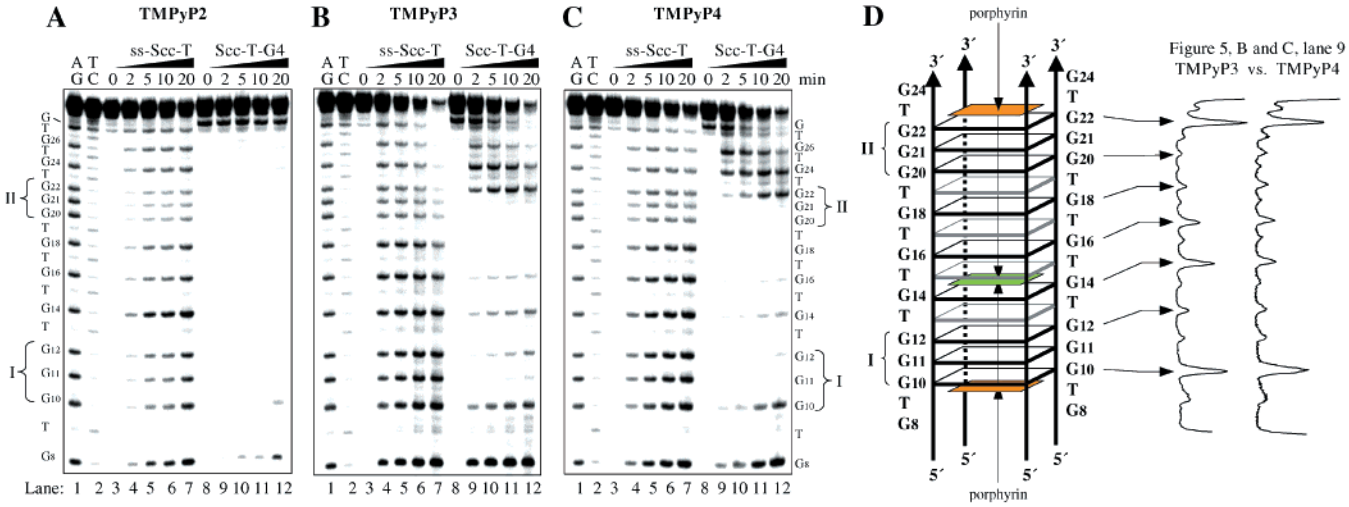


**Figure 5.** Time-dependent photocleavage of ss-Scc-T and Scc-T−G4 by TMPyP2 (A), TMPyP3 (B), and TMPyP4 (C). Lanes 1 and 2 are Maxam−Gilbert sequencing reactions. Lanes 3−7 are photocleavage assays of ss-Scc-T in TE buffer (pH 8.0). Lanes 8−12 are photocleavage assays of Scc-T−G4 in TE buffer containing 100 mM $K^+$. The positions of the guanine residues are numbered relative to the 5′-end. (D) Model for the porphyrins interacting with TMPyP3 and TMPyP4. TMPyP3 and TMPyP4 porphyrin molecules (orange) stack externally to G-tetrads at the two ends of Scc-T−G4, and possibly between the G- and T-tetrads formed by $T_{13}$, $G_{14}$, $T_{15}$, $G_{16}$, $T_{17}$, and $G_{18}$ (e.g., green). To the right of the model are the band peaks scanned from lane 9 in (B) (TMPyP3) and (C) (TMPyP4). To compare the cleavage of TMPyP3 and TMPyP4 in the region between $G_{12}$ and $G_{20}$, scanned peaks were normalized at $G_{22}$. TMPyP3 showed somewhat stronger cleavage at $G_{14}$ and $G_{16}$ than TMPyP4.

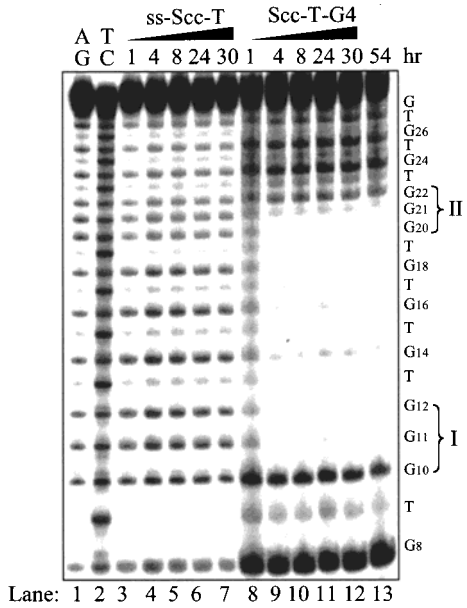


**Figure 6.** Effect of elongated incubation of TMPyP4 with ss-Scc-T and Scc-T−G4 on photocleavage patterns. Lanes 1 and 2: Maxam−Gilbert sequencing reactions. Lanes 3−7: ss-Scc-T was incubated with TMPyP4 for 1, 4, 8, 24, and 30 h in TE buffer (pH 8.0) before being subjected to photocleavage for 15 min. Lanes 8−13: Scc-T−G4 DNA was incubated with TMPyP4 for 1, 4, 8, 24, 30, or 54 h in TE buffer (pH 8.0) containing 100 mM $K^+$ before being subjected to photocleavage for 15 min.

were also greatly reduced for both TMPyP3 and TMPyP4 relative to ss-Scc-T. TMPyP4 had little cleavage at these residues, while TMPyP3 showed some cleavage, but this was much weaker than at the guanine residues located at the 5′- and 3′-ends (Figure 5B and C, lanes 8−12, and Figure 5D). This finding suggests the formation of a less stable G-quadruplex structure in this region. The apparent different binding affinities of TMPyP3 and TMPyP4 at these sites may partially explain their different inhibitory activities on the unwinding of Scc-T−G4 by Sgs1p (see Discussion).

**Molecular Dynamics Comparison of TMPyP4 in an Intercalated versus External Binding Mode to the Monomolecular Antiparallel G-Quadruplex Shows That the TMPyP4 Intercalation Complex Is a Less Favored Binding Mode.** The NMR structure of the d($AG_3[T_2AG_3]_3$) antiparallel G-quadruplex[6a] was used in the modeling studies. Four different molecules were subjected to molecular dynamics: the noncomplexed d($AG_3[T_2AG_3]_3$) quadruplex ($K^+$ complex), a TMPyP4 externally bound species (G1 complex), a TMPyP4 intercalated species (G2 complex), and TMPyP4. The $K^+$, G1, and G2 complexes are shown in Figure 7B. Although neither the externally bound nor the intercalated species can be directly compared to that formed with parallel G-quadruplex used in the experimental part of this study, it is likely that they have many energetic similarities, particularly the intercalated species. Moreover, we have demonstrated that irrespective of whether the G-quadruplex is the tetramolecular or monomolecular species, TMPyP4 always appears to bind in the external mode (Figures 5 and 6).[18c] Nevertheless, some caution is necessary in extrapolating results from this molecular modeling study on the monomolecular antiparallel G-quadruplex complex to other structures, such as the parallel G-quadruplex structure.

**(1) TMPyP4.** The energetics (Table 1) and conformational sampling (Figure 7C, magenta) of TMPyP4 showed that it rapidly stabilized in a 2.02-ns simulation. The 4-methylpyridinium groups fluctuate about a conformation that is roughly perpendicular (90 ± 20°) to the plane of the porphyrin ring system. This conformation disrupts the conjugation between the porphyrin ring system and the four 4-methylpyridinium groups but reduces the nonbonded (van der Waals (vdw) and electrostatic) interactions between the 2,6-pyridinium positions and the $\beta$-position of the porphyrin core. The chloride ions are randomly dispersed throughout the simulation box and are not closely associated with the 4-methylpyridinium groups due to the effective screening of the high dielectric water environment.

**(2) d($AG_3[T_2AG_3]_3$) Antiparallel G-Quadruplex ($K^+$ Complex).** The energetics (Table 1) and conformational sampling (Figure 7C, red) took longer to stabilize for the G-quadruplex potassium ion system compared to TMPyP4. The RMSD plot (Figure 7C, red) shows that after an initial drift away from the

**Table 1.** Average Energy (in kcal/mol)[a]

| | TMPyP4 | $K^+$ | G1 | G2 | G1 − free[b,c] | G2 − free[b,c] | G1 − G2[d] |
|---|---|---|---|---|---|---|---|
| | | | | Vacuum Energy | | | |
| DNA total | 0.00 | −1404.28 | −1280.51 | −1310.31 | 123.77 | 93.97 | 29.80 |
| internal | 0.00 | 992.15 | 1014.61 | 1007.45 | 22.46 | 15.30 | 7.16 |
| van der Waals | 0.00 | −316.95 | −261.39 | −225.95 | 55.56 | 91.00 | −35.44 |
| electrostatic | 0.00 | −2079.51 | −2034.00 | −2092.07 | 45.51 | −12.56 | 58.07 |
| TMPyP4 total | 80.32 | 0.00 | 83.10 | 85.44 | 2.78 | 5.12 | −2.34 |
| internal | 97.38 | 0.00 | 96.58 | 95.82 | −0.80 | −1.56 | 0.76 |
| van der Waals | −2.26 | 0.00 | 0.22 | 2.09 | 2.48 | 4.35 | −1.87 |
| electrostatic | −14.79 | 0.00 | −13.70 | −12.48 | 1.09 | 2.31 | −1.22 |
| | | | | Interaction Energy | | | |
| DNA−TMPyP4 | 0.00 | 0.00 | −210.39 | −194.93 | −210.39 | −194.93 | −15.46 |
| DNA−$H_2O$ | 0.00 | −3007.82 | −3037.87 | −2969.93 | −30.05 | 37.89 | −67.94 |
| DNA−$K^+$ | 0.00 | −610.74 | −503.02 | −528.29 | 107.72 | 82.45 | 25.27 |
| $K^+$−TMPyP4 | 0.00 | 0.00 | 19.76 | 27.96 | 19.76 | 27.96 | −8.20 |
| $H_2O$−TMPyP4 | −226.50 | 0.00 | −252.30 | −279.92 | −25.80 | −53.42 | 27.62 |
| Cl−TMPyP4 | −18.18 | | | | | | |
| $\Delta H°$[e] | | | | | −12.21 | −0.96 | |
| $\Delta\Delta H°$[f] | | | | | | | −11.25 |

[a] The energies were averaged over the 4040 (TMPyP4) or 6040 ($K^+$, G1, G2) structures (save at 0.5-ps intervals) from each of the MD simulations. [b] Free = TMPyP4 + $K^+$. [c] Negative values favor the DNA−TMPyP4 complex. [d] Negative values favor the G1 complex. [e] $\Delta H° = (\text{DNA}_{\text{total energy}} + \text{TMPyP4}_{\text{total energy}} + \sum\text{interaction energies})_{\text{bound}} - (\text{DNA}_{\text{total energy}} + \text{TMPyP4}_{\text{total energy}} + \sum\text{interaction Energies})_{\text{unbound}}$. [f] $\Delta H° = \Delta H°_{G1} - \Delta H°_{G2}$.

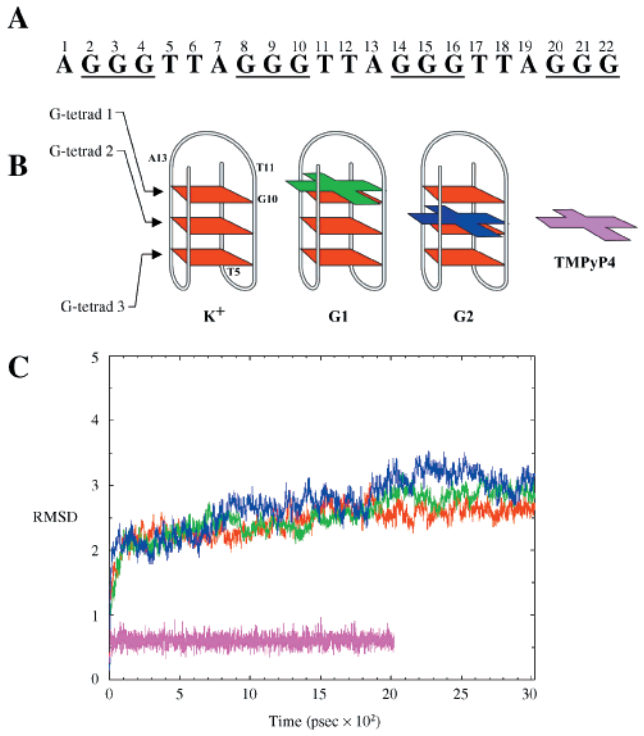


**Figure 7.** (A) Numbering of the sequence used in molecular modeling studies. (B) Cartoons of the G-quadruplex with $K^+$ ($K^+$), the G1 complex (G1), the G2 complex (G2), and TMPyP4. (C) Time evolution of the all-atom mass weighted root mean square difference (Å) between the structures generated during the MD simulation on the $K^+$ (red), G1 (green), and G2 (blue) complexes and TMPyP4 (magenta), at 0.5-ps time points. The $K^+$ MD-generated structures are compared with the NMR structure from 143D.pdb. G1 and G2 MD-generated structures are compared with the "model-built" structure of the G1 or G2 complex. The model-built structure is the starting point for the MD simulation. TMPyP4 MD-generated structures are compared with the energy minimized structure of TMPyP4.

NMR structure[6a] (uncorrected structure, 143D.pdb) the simulation stabilized for ∼1 ns and then drifted to a second conformational state. The major difference between the two states is in the conformation of the large lateral loop and to a lesser extent the diagonal loop. In particular, the relative position of $T_5$ to the G-quadruplex core has changed (Figure S2, Supporting Information). The large calculated thermal factors (Figure S5, red; Supporting Information) for these residues reflect this mobility. An examination of the six NMR structures provided in the 143D.pdb file confirms that these loops are highly mobile and adopt a number of different conformations beyond and including the ones observed in this MD study. An analysis of the conformational parameters (Figure S6, red; Supporting Information) shows that the internal conformational sampling observed in the MD structures reflects the experimental values. Also consistent with the NMR study, the sugars predominantly exist in the C2′-endo conformation, with the exception of $G_{10}$ which prefers the C3′-endo conformation (Figure S2, Supporting Information). The $G_{10}$ C3′-endo pucker allows $G_{10}$ to move slightly out of the plane with respect to the other bases in tetrad 1. This out-of-plane movement shortens the distance that the diagonal loop must traverse from ∼20.4 to ∼18.0 Å and allows the diagonal loop to move more freely. Additionally, the hydrogen bond distance (Figure S7, red, Supporting Information; and Figure 8) between the bases within the G-tetrads are reproduced. The shoulder that is observed on the high side of the $O_6 \leftrightarrow H_1$, $N_7 \leftrightarrow H_{21}$, and $O_6 \leftrightarrow H_{21}$ and the low side of $N_7 \leftrightarrow H_1$ (Figure S6; Supporting Information) arises when one or more bases within a tetrad shift to form bifurcated hydrogen bonds[35] (Figure 8). This shift reduces the size of the hole down the center of the quadruplex and is more frequently observed in MD studies where the potassium ions are replaced with smaller sodium ions (data not shown). While the bifurcated hydrogen-bonding network decreases the size of the hole down the center of the quadruplex (i.e., the four guanine $O_6$ carbonyl oxygens move closer together), it increases the distance between opposing grooves. For example, the distance between $H_{21}$ of the 2-amino groups in opposing grooves of the canonical hydrogen-bonded G-tetrad fluctuates between 12.50 and 14.00 Å (Figure 8A), while the bifurcated hydrogen-bonded tetrad fluctuates between 13.00 and 15.00 Å (Figure 8B).

**(3) $d(AG_3[T_2AG_3]_3)$ Antiparallel G-Quadruplex/TMPyP4 (G1 Complex).** As in the $K^+$ complex, the G1 complex exhibits more than one conformational state. In this complex residues $A_1$ on the 5′-terminal end and $A_{13}$ of the diagonal loop are

(35) Spackova, N.; Berger, I.; Sponer, J. *J. Am. Chem. Soc.* **1999**, *121*, 5519−5534.

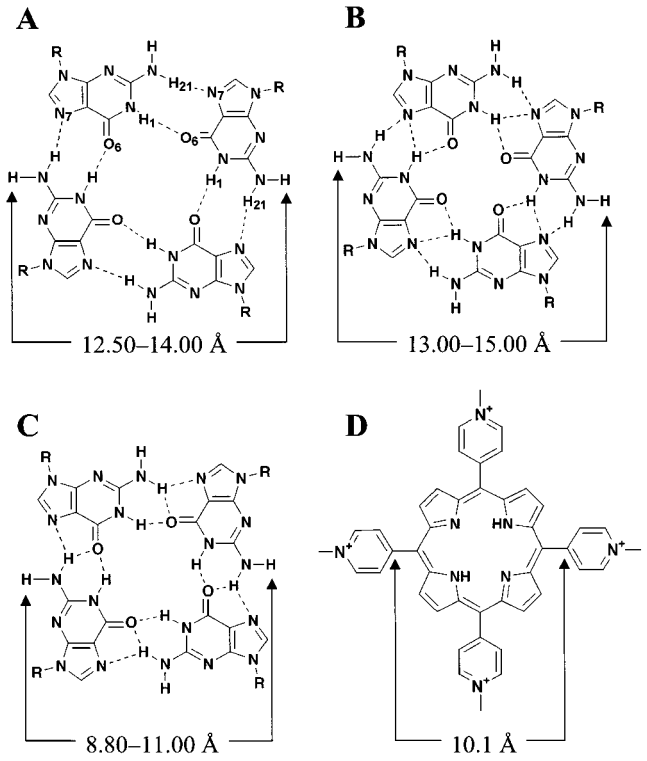


**Figure 8.** Distances across the differently hydrogen-bonded G-tetrads. These fluctuate among (A) 12.50−14.00 Å for the normally hydrogen-bonded tetrad, (B) 13.00−15.00 Å for the bifurcated hydrogen-bonded tetrad, (C) 8.80−11.00 Å for the narrow bifurcated hydrogen-bonded tetrad, and (D) TMPyP4. The distance across the porphyrin core of TMPyP4 is 10.1 Å.

rotated away from tetrad 1 and into the solvent (Figure S3; Supporting Information) to make room for TMPyP4 to reside between the diagonal loop and tetrad 1. This results in an increase in the conformational flexibility of A1 and the entire diagonal loop (Figure S5, green; Supporting Information). Despite the increase in the calculated thermal factors for the diagonal loop, all of the residues in the three G-tetrads remain stable (small thermal factors) and the model continues to sample the conformational parameters defined by NMR (Figure S6, green; Supporting Information). The size of the TMPyP4 porphyrin core (10.1 Å, Figure 8D) is slightly smaller than the canonical G-tetrad (13.2 Å). The difference in size is relieved by the way that TMPyP4 fits into the binding site. The TMPyP4 center of mass is displaced from the G-quadruplex helical axis by ∼2.5 Å. This allows the 4-methylpyridinium group that resides in the minor groove to move farther out of the groove and away from the 2-amino group of G22. The 4-methylpyridinium group that resides in the opposite groove is pulled deeper into the major groove and partially sits over G2 and against G10. This is made possible due to the preferred G10 C3′-endo pucker, which allows G10 to move out of the plane with respect to the other bases in tetrad 1 (Figures S2 and S3; Supporting Information). The remaining two 4-methylpyridinium groups resides in the medium-sized grooves and place structural restrictions on tetrad 1, which reduces the sampling frequency of the larger bifurcated hydrogen-bonded structure. Interestingly, this reduction is accompanied by more frequent sampling of the bifurcated hydrogen-bonded structure by tetrads 2 and 3 (Figure 8 and Figure S7, green; Supporting Information) and at least partially accounts for the slight increase in the thermal factors for residues 14−16 and 20−22 (Figure S5, green; Supporting Information). It should be noted that this model is consistent with the TMPyP4 photocleavage of $d(TTAGGG)_4$[18c] and provides a structural explanation for the weaker cleavage observed for G6 relative to G1, G7, and G12 (see Figure 1 of ref 21c; G6 of Figure 1[18c] is equivalent to G10 of this study).

The opening of the DNA conformation to accommodate TMPyP4 reduces the number of intermolecular contacts between the residues in the diagonal loop and tetrad 1 and decreases the energetic stability of the DNA (Table 1, G1 − free) by 123.77 kcal/mol compared to the DNA in the $K^+$ model. The energy loss is nearly evenly spread among the internal, vdw, and electrostatic terms. In addition, the bound conformation of TMPyP4 is less stable by 2.78 kcal/mol. In the bound conformation, the 4-methylpyridinium groups rotate to 72.5 ± 15° to mold to the DNA grooves. While this increases the conjugation of the pyridinium groups with the porphyrin ring system and lowers the internal energy of the system, it increases the vdw and electrostatic repulsion between the 2,6-pyridinium positions and the $\beta$-position of the porphyrin core. There is also a loss in the DNA−potassium and TMPyP4−potassium attractive interaction terms. The loss in energetic stability for these interaction terms is largely due to the reduction in the number of potassium ions in the G1 complex (17 ions) versus the $K^+$ complex (21 ions) and the introduction of TMPyP4 into the G1 complex. It should be noted that, in both the $K^+$ and G1 simulations, potassium ions move freely in and out of all four of the DNA grooves. However, the resonance time is longer in the small and two medium-sized grooves of the G-quadruplex relative to the large groove. The loss in energetic stability discussed above is offset by the DNA−$H_2O$, DNA−TMPyP4, and $H_2O$−TMPyP4 interaction energy terms (Table 1). In the G1 complex residues, A1 and A13 are more exposed to the solvent relative to $K^+$ complex, which allows water molecules greater access to hydrogen bond with $N_1$, $N_3$, $N_7$, and the 6-amino group. The strong DNA−TMPyP4 interaction energy arises from both vdw and electrostatic interactions. The porphyrin ring makes vdw contact with tetrad 1 on one face and the diagonal loop on the other face. The four 4-methylpyridinium groups also make favorable vdw contacts with the four grooves, as well as with G2 and G10 of the G-quadruplex. In addition, the cationic charges on the pyridinium groups are in close contact (5.5 ± 3.5 Å) with the anionic charges on the phosphate groups of tetrad 1 and the three phosphate groups in the diagonal loop. The binding of TMPyP4 to the DNA partially buries the hydrophobic porphyrin core in the DNA, leaving only the four charged 4-methylpyridinium groups to interact with the water. Thus, the observed decrease in the $H_2O$−TMPyP4 interaction energy is best thought of as the loss of high-energy water molecules from the solvation shell around the TMPyP4 porphyrin core.

By summing up the different components, the enthalpy of binding ($\Delta H°$, Table 1) for the G1 system is predicted to be −12.21 kcal/mol. If we use the $\Delta G°$ determined for TMPyP4 at saturation binding with $d(AG_3[T_2AG_3]_3)$ in the $K^+$ buffer[21] (Table 2), then the entropy ($T\Delta S°$) term of the free energy of binding is predicted to be −6.11 kcal/mol. The negative $\Delta H°$ and $T\Delta S°$ ($\Delta S° = -2.05 \times 10^{-2}$ kcal/K·mol at 298 K) terms are consistent with an enthalpy-driven binding mechanism where the favorable $\Delta H°$ term is countered by an unfavorable $\Delta S°$ term.

**(4) $d(AG_3[T_2AG_3]_3)$ Antiparallel G-Quadruplex/TMPyP4 (G2 Complex).** The G2 complex is thermally the least stable of the three G-quadruplex systems (Figure S5, blue; Supporting Information). In the G2 complex, TMPyP4 sits between tetrads 1 and 2 toward the center of the G-quadruplex (Figure 7B). However, due to the difference in the size between the G-tetrads

**Table 2.** Energy Parameters for TMPyP4 Binding to DNA Quadruplexes[a]

| host DNA | $N$[b] | $K_b$ ($\times 10^4\,M^{-1}$) | $\Delta G°$ (kcal/mol) | $\Delta H°$ (kcal/mol) | $T\Delta S°$ (kcal/mol) |
|---|---|---|---|---|---|
| | | $K^+$ Buffer[c,d] | | | |
| $d(G_2T_2G_2TGTG_2T_2G_{2)}$ | 1 | 17.8 | −7.2 | −9.6 | −2.4 |
| $d(AG_3[T_2AG_3]_3)$ | 2 | 2.8 | −6.1 | −4.2 | +1.9 |
| $d(T_4G_4)_4$ | 3 | 7.7 | −6.7 | −9.1 | −2.4 |
| | | $Na^+$ Buffer[a] | | | |
| $d(AG_3[T_2AG_3]_3)$ | 1 | 3.3 | −6.2 | −6.8 | −0.6 |
| $d(T_4G_4)_4$ | 1 | 162 | −8.5 | −6.7 | +1.8 |
| $d(T_4G_4)_4$ | 2 | 4.4 | −6.3 | −25.3 | −19.0 |
| | | Calculated | | | |
| G1 complex $d(AG_3[T_2AG_3]_3)$ | 1 | | −6.1[e] | −12.21 | −6.11 |
| G2 complex $d(AG_3[T_2AG_3]_3)$ | 1 | | −6.1[e] | −0.96 | +5.14 |
| average[f] | 2 | | −6.1[e] | −6.585 | +0.485 |

[a] The thermodynamic parameters were calculated using the following relationships: $\Delta G°= \Delta H° - T\Delta S°= -RT \ln K_b$, where $R = 1.987\,17 \times 10^{-3}$ kcal/K·mol, $T = 298$ K, and $K_b$ = [free ligand]/[bound ligand]. [b]Number of TMPyP4 molecules bound per quadruplex at saturation. [c] The data for the $K^+$ and $Na^+$ buffer systems were determined by isothermal titration calorimetry.[21] [d]This set of isothermal titration calorimetry data assumes a single set of identical binding sites. [e]The experimental $\Delta G°$ determined by isothermal titration calorimetry[21] for the $d(AG_3[T_2AG_3]_3)$ complex in $K^+$ buffer was used to determine the calculated $T\Delta S°$. [f]Average of the thermodynamic parameters for the G1 and G2 complexes.

and the porphyrin core (Figure 8), this is less than an optimal fit. Within the first few picoseconds of the MD simulation, the hydrogen-bonding network for tetrad 1 shifts to reduce the distance between the 2-amino groups of guanine in opposing grooves (Figure 8C). During the remainder of the MD simulation, tetrad 1 continues to shift back and forth between the normal (Figure 8A) and the narrow (Figure 8C) hydrogen-bonded networks, producing the high thermal factors observed for these residues (Figure S5, blue; Supporting Information). During the course of the simulation, residue $G_{14}$ or $G_{22}$ is periodically displaced to leave a short-lived triad. This displacement is reflected in the small population of abnormally long and short hydrogen bond distances observed for $O_6 \leftrightarrow H_1$, $N_7 \leftrightarrow H_{21}$, and $N_7 \leftrightarrow H_1$ and $O_6 \leftrightarrow H_{21}$, respectively (Figure S7, blue; Supporting Information). Tetrads 2 and 3 remain reasonably stable throughout the simulation; however, there is a noticeable increase in the number of sugar pucker transitions between the 2′-endo and 3′-endo conformations (Figure S6, blue; Supporting Information). Despite the ongoing structural changes in tetrad 1, the four grooves of the DNA remained well defined and the DNA conformational parameters continued to sample the NMR-defined conformational space.

The well-defined grooves and intercalation cleft in the G2 complex impose larger conformational constraints on the rotation ($64.3 \pm 25°$) of the four 4-methylpyridinium groups attached to the porphyrin core of TMPyP4 relative to the G1 complex. Just as in the G1 complex, this reduces the energetic stability of TMPyP4 (Table 1) by increasing both the vdw and electrostatic repulsion terms. The DNA is also less stable than in the $K^+$ form. The insertion of TMPyP4 into G2 forms an intercalation site by moving tetrads 1 and 2 away from each other. This disrupts the $\pi$-stacking between the tetrads and results in a 91 kcal/mol loss in the vdw attraction term and an increase in the internal strain energy. The loss in energetic stability is somewhat offset by a decrease in the electrostatic repulsion between the phosphate groups of tetrads 1 and 2. In the G2 complex, the four spines of hydration in the grooves of the G2 complex are disrupted relative to either the $K^+$ or G1 complex, which accounts for the reduction in the DNA−$H_2O$ interaction energy. The DNA−$K^+$ interaction energy is less favorable compared to the $K^+$ complex but more favorable relative to the G1 complex. In the G1 complex, TMPyP4 resides at one end of the quadruplex and partially neutralizes the charge on the six phosphate groups in the diagonal loop and tetrad 1. However, in the G2 complex, TMPyP4 is near the center of the quadruplex and only partially neutralizes the charge on the four phosphate groups that reside between tetrads 1 and 2. This difference not only reduces the attractive electrostatic interactions between the DNA and TMPyP4, for G2 relative to G1, but allows more potassium ions to come into closer contact with both the DNA and TMPyP4. This results in the stabilization of the DNA−$K^+$ and destabilization of the $K^+$−TMPyP4 interaction relative to the G1 complex. In the G2 complex, the hydrophobic porphyrin core of TMPyP4 is completely protected from the $H_2O$ environment, which further lowers the $H_2O$−TMPyP4 interaction energy, compared to the TMPyP4 or G1 simulations.

The enthalpy of binding ($\Delta H°$, Table 1) for the G2 complex is predicted to be −0.96 kcal/mol. Assuming the G1 and G2 binding modes have nearly identical $\Delta G°$ values under the $K^+$ buffer conditions,[21] then the entropy ($T\Delta S°$) component of the free energy of binding is predicted to be +5.14 kcal/mol ($\Delta S° = +1.72 \times 10^{-2}$ kcal/K·mol at 298 K). In sharp contrast to the G1 binding model, the $\Delta G°$ (Table 2) for the G2 complex is dominated by the large favorable $T\Delta S°$ term and complemented by a very small favorable $\Delta H°$ term.

## Discussion

**Structurally Similar Porphyrins Show Dramatic Differences in Their Abilities To Facilitate the Formation of G-Quadruplexes and Stabilize Them to Helicase Unwinding.** The gel shift data (Figure 1) showed that, among the three porphyrins, only TMPyP3 was able to promote the formation of a parallel tetrameric G-quadruplex. Under the buffer conditions (1× TE, pH 8.0, and 100 mM $K^+$) used in the gel shift experiments, DNA oligomers containing four repeats of d(TTAGGG) are contained in an equilibrium of at least four different types of G-quadruplexes (Scheme 1). According to the mobility gel shift assay, most of the G-quadruplexes are in the form of intramolecular antiparallel quadruplexes, while the amount of dimeric and tetrameric quadruplexes is very small (lane 1 in Figure 1). The fact that TMPyP3 is able to dramatically increase the proportion of parallel tetrameric G-quadruplex (lane 9 in Figure 1) may be due to the preferential stabilization of the parallel G-quadruplex by TMPyP3, in contrast to TMPyP4. This conclusion is supported by the observation in the helicase assay that TMPyP3 prevents the

unwinding of parallel G-quadruplex by Sgs1p to a much greater extent than TMPyP2 and TMPyP4 (Figure 2). TMPyP2 showed no activity in either the facilitation of formation of G-quadruplexes or the inhibition of unwinding in helicase assays (Figures 1−3), indicating that this porphyrin does not appreciably interact with either parallel or antiparallel G-quadruplexes. In contrast, TMPyP4 showed some facilitation or inhibitory activity in both assays (Figures 1 and 2). In the helicase assay using antiparallel dimeric G-quadruplexes as helicase substrate, TMPyP4 showed higher Sgs1p inhibitory activity than TMPyP3, suggesting that TMPyP4 might be more specific to antiparallel G-quadruplexes (Figure 3).

TMPyP2, TMPyP3, and TMPyP4 are all positional isomers. The only structural difference among these three porphyrin analogues is the position of the *N*-methyl group on the pyridyl ring relative to its connection to the porphine core (Chart 1). The different position of the *N*-methyl group determines the free rotation of the pyridyl rings at the meso positions and the relative dihedral angles of the porphine core and pyridyl groups. In turn, this must affect their interaction with the G-quadruplexes. It is possible that TMPyP3 fits the pockets between the end G-tetrads and the loops in a parallel G-quadruplex considerably better than TMPyP4, whereas TMPyP2 does not fit any site in the parallel G-quadruplex.

**Photocleavage Experiment Studies Suggest That Porphyrin Molecules Favor Binding to G-Quadruplex Structures through External Stacking to the G-Tetrads over Binding through Intercalation between the G-Tetrads.** Two models have been proposed for the interaction of porphyrin molecules with G-quadruplex structures. One is the tetrad intercalation model, which postulates that the porphyrin molecules intercalate between two successive G-tetrads. This model is mainly based on the stoichiometry data obtained from isothermal titration calorimetry and molecular modeling studies.[21] The second model, which is based on photocleavage data of antiparallel monomeric G-quadruplex DNA, proposes that porphyrins externally stack to the two ends of the G-tetrad.[20] The photocleavage data on parallel G-quadruplex DNA reported here showed that when the single-stranded Scc-T molecules associate together to form a G-quadruplex structure, TMPyP3 and TMPyP4 cleavage at the inner G-tetrads ($G_{11}$ and $G_{21}$) of the proposed tetrameric G-quadruplex is almost completely diminished (Figure 5). This result suggests that the TMPyP3 and TMPyP4 molecules do not appreciably interact with the inner G-tetrads under the experimental conditions reported here, which is consistent with the external stacking model. The time course incubation experiment (Figure 6) also suggests that the intercalation of porphyrin molecules between two G-tetrads is neither kinetically nor thermodynamically favored. This finding would therefore apparently argue against the intercalation model, which would predict the cleavage of guanines located in the inner G-tetrads.

**Photocleavage Data Suggest That Isolated Guanines between the Two G-Clusters Form G-Tetrads, Which May Stack with the Secondary Structures Formed by Adjacent Thymines.** Predictions for G-quadruplex formation suggest that the guanines located between the two guanine clusters ($G_{14}$, $G_{16}$, $G_{18}$) would not be involved in the G-quadruplex formation and therefore should be as accessible to the porphyrins as those ($G_{24}$, $G_8$) at the 3′- and 5′-ends of the sequence. However, we observed a significantly reduced cleavage by TMPyP3 and TMPyP4 with these guanines (Figure 5B and C, lanes 8−12). This result suggests that these guanines might be involved in some sort of higher order structure. One possibility we favor is that the tightly tied ends (two G-tetrad stacks) drive the guanines between them to associate with the corresponding guanine residues from adjacent DNA strands in order to form tetrad structures. However, since a single G-tetrad may not be stable enough, it may need to stack with the adjacent thymine residues in order to exist in solution. The stabilization role of thymines in the dimeric quadruplex has been noted previously.[36] Thymines located adjacent to G-tetrads are usually found to form hydrogen bonds with thymines from adjacent DNA strands and then to stack to proximate G-tetrad structures. As has been shown previously,[37] the thymine residue in the parallel G-quadruplex formed from d(GGGGTGGGG) is not accessible to $KMnO_4$ cleavage, suggesting the involvement of this thymine in a higher order structure. A recent NMR study of parallel G-quadruplex structures formed from the sequence d(TGGTGGC) revealed that the thymine residue in the middle of the sequence is involved in T-tetrad formation.[38] This T-tetrad stacks with the adjacent G-tetrads and contributes to the overall stabilization of the quadruplex, and it also causes a small underwinding of the right-handed quadruple helix.[38] On the basis of our photocleavage results and these published data, we propose that the thymines (Figure 5D, $T_{13}$, $T_{15}$, $T_{17}$, and $T_{19}$) located between the two G-clusters associate with corresponding thymine residues from other strands to form T-tetrad structures, and these T-tetrads stack with adjacent G-tetrads to form a stable quadruplex structure. However, the stacking between T-tetrads and G-tetrads is not as stable as that between consecutive G-tetrads, and the quadruple helix might be more easily distorted in this region to accommodate the porphyrin. Therefore, porphyrin molecules might still have limited access to the G-tetrads in this region. The intercalation of porphyrin molecules between G-tetrads and T-tetrads increases the overall stability of the parallel quadruplex structure. The higher cleavage activity of TMPyP3, compared to TMPyP4, in this region indicates that TMPyP3 is probably more stable at these G−T steps than TMPyP4, and this might also contribute to the higher stabilization effect of TMPyP3 over TMPyP4 that we observed in the Sgs1p unwinding assay.

**Molecular Modeling of TMPyP4 in an Intercalated versus External Binding Mode in Monomolecular G-Quadruplex Structures Predicts Why the External Binding Mode Is Favored.** Haq and co-workers[21] recently reported a study on the energetics of the binding interaction of TMPyP4 with the three DNA quadruplexes listed in Table 2 ($d(G_2T_2G_2TGTG_2T_2G_2)$, $d(AG_3[T_2AG_3]_3)$, and $d(T_4G_4)_4$) using isothermal titration calorimetry. The binding stoichiometry was found to be one porphyrin per number of G-tetrads minus one in the $K^+$ buffer and one porphyrin per number of G-tetrads minus two in the $Na^+$ buffer. The $K^+$ buffer binding thermodynamic parameters were best fitted using a model that assumed a single set of identical binding sites. However, the binding behavior in the $Na^+$ buffer showed a single high-affinity site and minor secondary binding sites. The interactions of TMPyP4 with each quadruplex are enthalpically driven under both the $K^+$ and $Na^+$ solution conditions. In the $K^+$ buffer, the momomeric antiparallel hairpin foldback (Table 2, $d(G_2T_2G_2TGTG_2T_2G_2)$), and the tetrameric parallel ($d(T_4G_4)_4$) structures, the $\Delta G°$ is unfavorably impacted by the negative $T\Delta S°$ entropic terms, whereas the positive $T\Delta S°$ term was favorable for the momomeric antiparallel diagonal foldback structure (Table 2, $d(AG_3[T_2AG_3]_3)$. This

(36) Keniry, M. A.; Owen, E. A.; Shafer, R. H. *Nucleic Acids Res.* **1997**, *25*, 4389−4392.

(37) Balagurumoorthy, P.; Brahmachari, S. K. *J. Biol. Chem.* **1994**, *269*, 21858−21869.

(38) Patel, P. K; Hosur, R. V. *Nucleic Acids Res.* **1999**, *27*, 2457−2464.

is contrary to what one would expect. Assuming nearly identical "intercalative binding sites," the $T\Delta S°$ term should become more favorable as the drug load increases and displaces a larger number of bound water molecules and counterions from the surface of the DNA. Nevertheless, the thermodynamic parameters are qualitatively in line with the parameters reported for the binding of ethidium bromide[39] and anthraquinone.[17g]

The enthalpy of binding ($\Delta H°$, Table 1) for the G1 complex is predicted to be −12.21 kcal/mol. Assuming $\Delta G° = -6.1$ kcal/mol (Table 2), determined for TMPyP4 at saturation binding with $d(AG_3[T_2AG_3]_3)$ in the $K^+$ buffer,[21] then the entropy ($T\Delta S°$) term of the free energy of binding is predicted to be −6.11 kcal/mol. The negative $\Delta H°$ and $T\Delta S°$ ($\Delta S° = -2.05 \times 10^{-2}$ kcal/K·mol at 298 K) terms are consistent with an enthalpy-driven binding mechanism where the favorable $\Delta H°$ term is countered by an unfavorable $\Delta S°$ term. These thermal dynamic parameters are consistent with the energetic terms. For example, in the external binding mode, residues $A_1$ and $A_{13}$ are displaced into the solvent to make room for TMPyP4 binding. This increases the surface area of the complex, which provides energetically favorable sites for water molecules to interact and reduces the $\Delta H°$ by lowering the DNA−$H_2O$ interaction energy. However, this comes at a cost in the $T\Delta S°$ term due to the ordering of the water molecules.

The enthalpy of binding ($\Delta H°$, Table 1) for the G2 complex is predicted to be −0.96 kcal/mol. Assuming that the G1 and G2 binding modes have near identical $\Delta G°$ values under the $K^+$ buffer conditions,[21] then the entropy ($T\Delta S°$) component of the free energy of binding is predicted to be +5.14 kcal/mol ($\Delta S° = +1.72 \times 10^{-2}$ kcal/K·mol at 298 K). In sharp contrast to the G1 binding model, the $\Delta G°$ for the G2 model is dominated by the large favorable $T\Delta S°$ term and complemented by a very small favorable $\Delta H°$ term. Contrary to the G1 complex, TMPyP4 intercalation disrupts the ordered spines of hydration in the four grooves of the quadruplex, resulting in a more favorable $T\Delta S°$ term at the expense of the DNA−$H_2O$ interaction energy and $\Delta H°$. This set of thermodynamic parameters is inconsistent with the published binding data for porphyrin and non-porphyrin quadruplex binding molecules.[40] This study suggests that TMPyP4 intercalation is a minor entropy-driven binding mode with a small but favorable enthalpy contribution. As such, this intercalation mode would make a minor exothermic contribution to the binding isotherms measured in the isothermal titration calorimetry experiment.

Individually, the thermodynamic parameters calculated for the G1 and G2 models are in disagreement with the results measured by Haq and co-workers[21] for the $K^+$-buffered TMPyP4/$d(AG_3[T_2AG_3]_3)$, $N = 2$ complex (Table 2). While the site of binding suggested by Haq et al. is conjecture based upon stoichiometry of porphyrins bound and number of available G-tetrads, the stoichiometry experimentally determined is more difficult to dismiss. Indeed, there is every reason to believe the proposed number of porphyrins bound per G-quadruplex structure. A major shortcoming of the model proposed by Haq et al. is that the intratetrad intercalation violates the neighboring base exclusion rule, which states that intercalation cannot occur at adjacent base pairs. Our photocleavage data suggest a single externally bound TMPyP4 in the $d(AG_3[T_2AG_3]_3)$ G-quadruplex, which is inconsistent with the $N = 2$ determined by Haq et al.[21] A possible way to reconcile our photocleavage data with the stoichiometry determined by Haq and co-workers is to assume that porphyrins in some binding sites (i.e., intercalation) are invisible when assayed by photocleavage. Since photocleavage by porphyrins requires an activated oxygen species, the sequestering of porphyrins within G-tetrads may either quench the photoactivating potential of TMPyP4 or exclude water from the site of porphyrin activation, thus resulting in a photochemically invisible species. Indeed, the molecular modeling of G2 demonstrates the exclusion of water. Therefore, we predict that two porphyrin molecules bind to $d(AG_3[T_2AG_3]_3)$, one at the energetically favored external binding site and the other at the less favored intercalation site. This is also in accord with averaging of the thermodynamic data from models G1 and G2 to predict the measured results for $d(AG_3[T_2AG_3]_3)$ in $K^+$ (see before). Furthermore, to reconcile the stoichiometry data of Haq et al. with our photocleavage and molecular modeling data reported here, we predict for $d(G_2T_2G_2TGTG_2T_2G_2)$ that the one TMPyP4 molecule would bind at the T−G quadruplex step and for $d(T_4G_4)_4$ that the three TMPyP4 molecules would bind such that one would be external at the T−G quadruplex step, the second by intercalation of a G−G quadruplex step, and the third intermolecularly by stacking between end-to-end parallel G-quadruplexes at noncovalently linked T−G steps. None of these modes of binding would violate the neighboring base exclusion rule, and they would be in agreement with the stoichiometry experimentally determined by Haq and co-workers.[21]

**Differential Binding of Structurally Similar Small Molecules to Different G-Quadruplexes Has Important Implications in the Development of Anticancer Agents That Target G-Quadruplex Structures.** Cellular events such as telomere maintenance, replication, transcription, and recombination have been suggested to involve G-quadruplex structures. These cellular events may involve different types of G-quadruplex structures.[2,14,23,29,41] How to achieve the selectivity against different types of G-quadruplexes and associated cellular events is a critical issue for therapeutic strategies targeting G-quadruplex structures. The data presented in this study suggest that G-quadruplex-interactive compounds with quite similar structures may exhibit differential effects in the facilitation of formation and stabilization of G-quadruplex structures. This conclusion is very important because it demonstrates that small molecules targeting G-quadruplex structures might be able to achieve the selectivity required for therapeutic intervention.[17]

**Acknowledgment.** This research has been supported by a grant from the National Institutes of Health (CA49751) and a National Cooperative Drug Discovery Group grant from the National Cancer Institute (CA67760). Dr. Richard J. Bennett of Harvard University kindly supplied the Sgs1 protein used in this study. We are grateful to the other members of the NCDDG team for insightful discussions, and to Dr. David M. Bishop for preparing, proofreading, and editing the final version of the manuscript and figures.

**Supporting Information Available:** Additional information as noted in text. See any current masthead page for ordering information and Web access instructions. This material is available free of charge via the Internet at http://pubs.acs.org.

JA002179J

(39) Guo, Q.; Lu, M.; Marky, L. A.; Kallenbach, N. R. *Biochemistry* **1992**, *31*, 2451−2455.

(40) Perry, P. J.; Reszka, A. P.; Wood, A. A.; Read, M. A.; Gowan, S. M.; Dosanjh, H. S.; Trent, J. O.; Jenkins, T. C.; Kelland, L. R.; Neidle, S. J. *J. Med. Chem.* **1998**, *41*, 4873−4884.

(41) (a) Zahler, A. M.; Williamson, J. R.; Cech, T. R.; Prescott, D. M. *Nature* **1991**, *350*, 718−720. (b) Sun, H.; Karow, J. K.; Hickson, I. D.; Maizels, N. *J. Biol. Chem.* **1998**, *273*, 27587−27592.